Single-Scattering Properties of Mixed-Phase Arctic Clouds at Solar Wavelengths: Impacts on Radiative Transfer

GREG M. MCFARQUHAR

Department of Atmospheric Sciences, University of Illinois at Urbana–Champaign, Urbana, Illinois

STEWART G. COBER

Cloud Physics and Severe Weather Research Division, Meteorological Service of Canada, Downsview, Ontario, Canada

(Manuscript received 8 December 2003, in final form 6 April 2004)

ABSTRACT

In situ observations of the sizes, shapes, and phases of Arctic clouds were obtained during the First International Satellite Cloud Climatology Project Regional Experiment (FIRE) Arctic Clouds Experiment (ACE). These particle distributions were then combined with a library of single-scattering properties, calculated using Mie theory and improved geometric ray optics, to determine the corresponding single-scattering properties (single-scattering albedo ω_0, phase function, and asymmetry parameter g) at solar wavelengths. During FIRE-ACE, mixed-phase clouds, where both water and ice were detected in 30 s of flight track, corresponding to 3.0-km horizontal extent, were observed in 33% of clouds. Because supercooled water drops generally dominate mass contents of these mixed-phase clouds, there is no statistically significant difference in the distributions of single-scattering properties of mixed-phase clouds compared to liquid-phase clouds, whereas those of ice crystals differ significantly. The average g for all mixed-phase clouds at visible wavelengths is $0.855 \pm .005$, similar to $0.863 \pm .007$ computed for water clouds, but higher than $0.767 \pm .007$ computed for ice clouds. Differences in g and ω_0 between mixed- and ice-phase clouds for near-infrared bands are also noted, whereas they are similar for mixed- and liquid-phase clouds.

Single-scattering properties computed using observations of mixed-phase clouds differ by more than 10% on average from those computed using a parameterization that describes the average fraction of water and ice in mixed-phase clouds. Simulations using a plane-parallel radiative transfer model show that these differences can cause top of the atmosphere albedos to vary between 6% and 100% depending on wavelength. However, when single-scattering properties are computed from observations over all phases (mixed, ice, and liquid), and average albedos are compared against those determined using the parameterized scattering properties, there is a difference of only 2% at visible wavelengths. Since observations show that the occurrence of phases is clustered, large-scale averages may not be representative of mixed-phase cloud climatic effects.

1. Introduction

Although regions at the poles are especially sensitive to climate change simulations, large uncertainties in the response of the Arctic to climate perturbations exist. Complex feedback mechanisms involving sea ice, snow cover, and clouds must be better understood and characterized before large disagreements between general circulation model (GCM) simulations (e.g., Lane et al. 2001) can be reduced and future predictions of climate change refined. A lack of comprehensive measurements of ice–ocean–atmosphere processes and cloud and radiation properties has limited progress on simulating feedback mechanisms. Recent observations obtained during the First International Satellite Cloud Climatology Project (ISCCP) Regional Experiment (FIRE) Arctic Clouds Experiment (ACE) and during the Surface Heat Budget of the Arctic Ocean Experiment (SHEBA) are being used to enhance our understanding of Arctic climate (Curry et al. 2001).

For Arctic clouds, Shupe et al. (2001) showed that retrieval techniques for all-ice and all-liquid clouds could be used only 34% of the time, suggesting mixed-phase clouds or overlapping clouds were present at other times. Understanding the properties of mixed-phase clouds is therefore critical for the Arctic environment because the modeled radiative properties of mixed-phase clouds differ substantially from those composed exclusively of liquid particles (Sun and Shine 1995). Gerber et al. (2000) and Garrett et al. (2001) used direct measurements of single-scattering cloud properties from a cloud integrating nephelometer (CIN) to illustrate these differences, finding larger values of asymmetry

Corresponding author address: Prof. Greg M. McFarquhar, Dept. of Atmospheric Sciences, University of Illinois, 105 S. Gregory Street, Urbana, IL 61801.
E-mail: mcfarq@atmos.uiuc.edu

parameters (g) for mixed- and liquid-phase clouds than for ice-phase clouds, with g depending on the relative amounts of water and ice. Not only do cloud radiative properties depend on the relative amounts of the phases, but also on their manner of spatial mixing (Sun and Shine 1994; Rotstayn et al. 2000).

There are few remote sensing techniques that accurately retrieve microphysical properties of mixed-phase clouds. For example, Hobbs et al. (2001) showed that liquid water contents (LWCs) could not be reliably retrieved using radar radiometer microwave techniques in mixed-phase Arctic clouds. On the other hand, Dong and Mace (2003) showed that microwave radiometers could be used to retrieve liquid water paths (LWPs) in most mixed-phase clouds observed at the Atmospheric Radiation Measurement Program's (ARM) North Slope of Alaska (NSA) site between May and September of 2000, suggesting that water droplets dominate the mass contents in mixed-phase clouds; they also found that surface solar transmission is dominated by water cloud optical depth. Thus, in situ measurements are needed to assess the fraction of liquid in mixed-phase clouds, the distributions of liquid and ice in the vertical, and how liquid and ice are distributed in different size particles. Such observations are somewhat scarce. Heymsfield (1993) reported climatologies of mixed-, ice-, and liquid-phase clouds as a function of temperature using data collected in the Soviet Union from 1953 to 1958 and compiled by Borovikov et al. (1963). Fleishauer et al. (2002) analyzed data collected in multilayered and single-layered mixed-phase clouds over the U.S. Great Plains during the Complex Layered-Cloud Experiments (CLEX-5), examining the vertical variation of ice and liquid water. Moss and Johnson (1994) analyzed the relative amounts of liquid and ice in mixed-phase clouds for maritime and continental air masses near the British Isles. Cober et al. (2001b) reported on characteristics of mixed-phase conditions observed during two midlatitude winter field programs. In the Arctic, in situ observations of mixed-phase clouds have been obtained during SHEBA and FIRE-ACE (Lawson et al. 2001; Rangno and Hobbs 2001; Hobbs et al. 2001; Korolev et al. 2003).

Early representations of liquid water fraction, f_1, as a function of temperature, derived for large-scale models had minimal basis in observation (e.g., Smith 1990). In situ observations have since been used to develop alternate representations for f_1 in terms of temperature (Moss and Johnson 1994; Bower et al. 1996; Boudala et al. 2002a). These representations significantly impact the simulation of climate. Gregory and Morris (1996) found that the radiation budget of the Met Office Unified Model depended on the temperature range over which mixed-phase clouds was assumed to exist, and Li and Le Treut's (1992) simulations were sensitive to the temperature threshold at which all clouds were assumed to be composed of ice. However, because factors other than temperature, such as cloud age and cloud-top temperature, affect f_1, it is likely that prognostic liquid and ice variables together with physically based parameterizations are needed to properly simulate mixed-phase clouds. Such models that allow explicit determination of liquid fraction in mixed-phase clouds have been developed (e.g., Lohmann and Roeckner 1996; Rotstayn et al. 2000) and are now used for some large-scale simulations. However, these schemes are not well evaluated against observations.

Fewer studies have used in situ observations to estimate radiative properties of mixed-phase clouds and the degree of mixing between phases. A better determination of how much water and ice contribute to cloud radiative properties is needed. Rotstayn et al. (2000) pointed out that their scheme for calculation of liquid fraction exhibited marked sensitivity to the assumed spatial mixing of water and ice. An alternate large-scale modeling approach (Del Genio et al. 1996) allowed only liquid or ice in a given grid box based on a random number and temperature-based liquid fraction.

This study uses in situ measurements obtained during FIRE-ACE to examine the nature of phase mixing and the contributions of water and ice to mixed-phase single-scattering properties. The roles of water and ice in determining the energy budget of this region are determined from radiative transfer simulations performed using single-scattering properties calculated using in situ observations. The remainder of the paper is organized as follows. Section 2 describes microphysical data collected during FIRE-ACE, and section 3 describes techniques used to compute cloud single-scattering properties. Section 4 identifies the roles of water and ice for determining single-scattering properties of mixed-phase clouds, and describes simulations conducted with a plane-parallel radiative transfer model. Section 5 discusses the significance of the findings.

2. Description of in situ microphysical data

a. Data overview

Instruments on board the National Research Council (NRC) Convair-580 (CV580) aircraft were used to collect microphysical data during FIRE-ACE in April 1998. Cober et al. (2001a,b) summarize the instrumentation and processing techniques; hence only the most salient features are described here. The CV580 was equipped with several Particle Measuring Systems, Inc. (PMS), probes that were used to measure the drop and ice crystal particle size distributions (PSDs) including a two-dimensional cloud (2DC) probe for PSDs between 125 and 800 μm, a two-dimensional precipitation probe (2DP: 800 to 6400 μm), a two-dimensional gray probe (2DG: 125 to 1600 μm), and two forward scattering spectrometer probes (FSSP-096: 3.5 to 45.5 μm and FSSP-124: 5 to 95 μm). Water content was measured with a SkyTech Research, Inc., Nezvorov LWC/total water content (TWC) probe (Korolev et al. 1998), and

a King LWC probe. A Rosemount icing detector was used to determine icing rate and to identify the presence of supercooled water drops. The FSSP and 2D probes covered the drop spectrum from 1 to 3000 μm and the ice crystal spectrum from 100 to 6400 μm from which properties of the PSDs could be determined.

Eighteen research flights were flown during FIRE-ACE representing over 69 h of flight time. In-cloud data were identified using a total water content threshold of 0.005 g m^{-3} and an FSSP concentration threshold of 1 cm^{-3}. There were 327 min of in-cloud observations, corresponding to low cloud coverage of approximately 8% given the over 68 h of flight time. This is partially related to the thresholds that are high enough that only denser clouds are included in the sample. Since these clouds are most significant radiatively, it is these clouds that are the subject of this study. By changing the FSSP concentration threshold to 0.1 cm^{-3}, the fraction of in-cloud observations increases to 16%. Similarly, by reducing the TWC threshold to 0.001 g m^{-3} and the FSSP threshold to 0.1 cm^{-3}, the fraction of in-cloud observations increases to 23%. The in-cloud conditions identified with the reduced cloud threshold values were primarily identified to represent glaciated clouds with low ice water contents.

b. Phase identification

Data from all in-cloud penetrations were analyzed at 30-s resolution to identify cloud phase and to determine PSDs following Cober et al. (2001a). Cloud regions were identified as liquid, mixed, or glaciated using a combination of observations from several instruments including the 2DC, 2DP, FSSPs, RID, King LWC, and Nevzorov LWC/TWC probes. Cober et al. (2001a) also provided an estimate of the errors inherent in using this collection of instruments to estimate the cloud phase.

From the in-cloud observations during FIRE-ACE, 33% were identified as mixed phase, 16% as liquid phase, and 51% as ice phase. The relative percentage of liquid, mixed, and glaciated conditions is sensitive to the cloud threshold used. For example, by changing the FSSP threshold to 0.1 cm^{-3} and the TWC threshold to 0.001 g m^{-3}, the relative fractions of liquid, mixed, and glaciated clouds changes to 0.16, 0.11, and 0.73, respectively. The temperatures of the mixed-phase clouds ranged from $-33°$ to -4.8°C, of the liquid-phase clouds from $-20.5°$ to -1.7°C, and of the ice-phase clouds from $-44°$ to -3.5°C. The mean and median LWCs for the liquid clouds were 0.11 and 0.05 g m^{-3}, while the mean and median LWCs for the mixed-phase clouds were 0.07 and 0.05 g m^{-3}. Conversely, the mean and median IWCs for the ice clouds were considerably lower, namely 0.02 and 0.012 g m^{-3}. This suggests that ice clouds are not as radiatively significant as water clouds with similar geometric thickness. Figure 1 shows the contribution of LWC to TWC, based on the Nezvorov probe measurements, for all clouds classified as

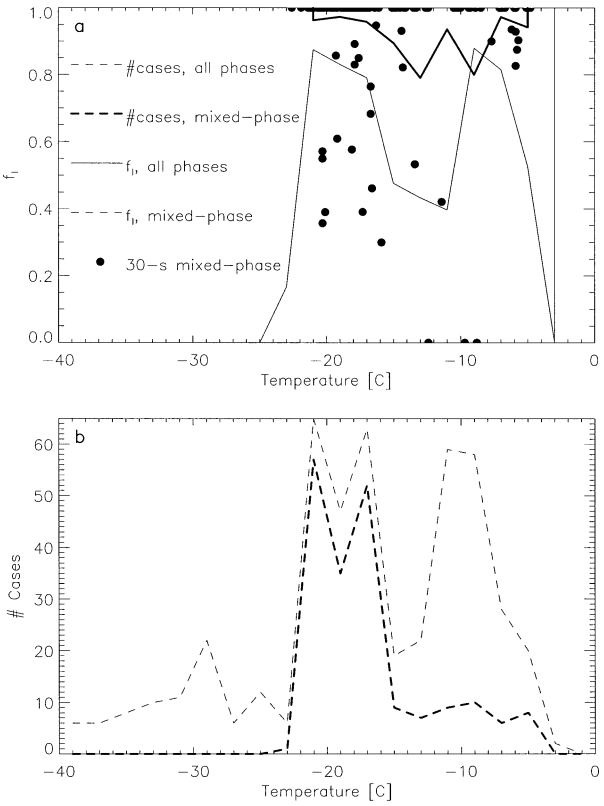

FIG. 1. Average fraction of liquid in mixed-phase clouds, f_1 = LWC/TWC, based on Nezvorov probe measurements and number of 30-s in-cloud time periods as function of temperature based on data acquired by the NRC Convair-580 during FIRE-ACE. Thin lines correspond to data collected in all (liquid, ice, and mixed phase) cloud types, whereas thick lines correspond to only mixed-phase clouds. Solid circles correspond to f_1 calculated for each 30-s period in mixed-phase cloud.

mixed phase (solid circles). The clustering of point about $f_1 = 1$ shows that for many cases, independent of temperature, ice water contents (IWCs) are too small to be explicitly measured by the Nezvorov probe; the conditions are known to be mixed because of the ice crystals observed with the 2DC. The thick solid line gives the average f_1 for all mixed-phase cases, which had mean and median IWCs of 0.003 and 0 g m^{-3}. The finding that mixed-phase clouds are generally dominated by the presence of one phase is not unique to FIRE-ACE. Cober et al. (2001a) and Korolev et al. (2003) have collected substantial data in mixed-phase clouds, showing that approximately 80% of mixed-phase clouds on average have ice fractions of either greater than 0.9 or less than 0.1.

Curves that give f_1 as a function of temperature in Fig. 1 vary according to whether all observations or just observations in mixed-phase clouds are used to construct them; the percentage of liquid in all clouds (thin lines) is lower than that in mixed-phase clouds (thick lines) because many clouds consisting only of ice are in the sample. Parameterizations used in some large-

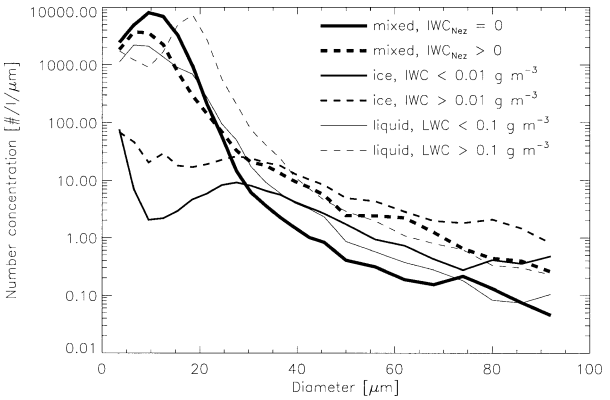

FIG. 2. Average PSDs measured by FSSP for different cloud phases identified by the Cober et al. (2001a) algorithm.

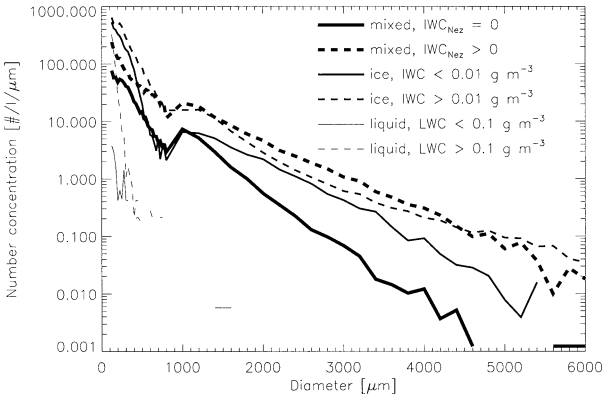

FIG. 3. Average PSDs measured by combination of 2D probes for different cloud phases identified by the Cober et al. (2001a) algorithm.

scale models (e.g., Smith 1990; Boudala et al. 2002a) give the fractional contributions of liquid water drops and ice crystals, and single-scattering properties are then computed by weighting single-scattering properties of water and ice according to the appropriate fraction. For example, Smith's (1990) formula give a liquid fraction of 0.54 at -6°C; then large-scale models, such as the National Center for Atmospheric Research's Community Climate Model Version 3 (CCM3), would weight single-scattering properties of water 54%, and those of ice 46%. These properties might differ considerably from a population that was, for example, 40% water clouds, 18% mixed-phase clouds, and 32% ice-phase clouds having the same average water fraction. Hence, FIRE-ACE microphysical data are used to calculate single-scattering properties of observed mixed-phase clouds, and to assess how the properties of these clouds differ from those of populations consisting of mixtures of liquid- and ice-phase clouds.

c. Derivation of particle-size distributions

To calculate single-scattering properties, estimates of PSDs for liquid- and ice-phase particles, as well as estimates of mass and projected area of liquid- and ice-phase particles are required. These are determined using data from the 2D probes, the Nezvorov probe, and the FSSP. The FSSP measures the sizes of particles by detecting the amount of light forward scattered by a particle falling through the probe's sample volume. FSSP data cannot typically be used quantitatively for glaciated conditions (Gardiner and Hallett 1985). Cober et al. (2001a) showed that the FSSP channels larger than 30 μm in diameter were heavily biased by responses to ice crystals (and hence inaccurate as an estimate of PSDs) whenever the ice crystal concentration for crystals larger than 125 μm exceeded approximately 1 L^{-1}. Further, they showed that FSSP data could be used to describe PSDs of mixed-phase clouds whenever the ice crystal concentrations were less than 1 L^{-1}. Approximately 71% of the FIRE-ACE mixed-phase clouds had ice crystal concentrations less than 1 L^{-1}, while 90% had ice crystal concentrations less than 2 L^{-1}. For those observations with ice crystal concentrations greater than 1 L^{-1}, interpretation of the FSSP measurements in channels larger than 30 μm as drops will result in an overestimate of the drop concentrations in these sizes.

FSSP data were examined to investigate these effects. As shown in Fig. 2, average PSDs measured by FSSPs in mixed-phase clouds (thickest lines) had peaks in number concentration between 5 and 15 μm, not differing significantly from PSDs measured in liquid clouds (thinnest lines). Patterns were similar for almost all 30-s average FSSP PSDs measured in mixed-phase clouds and regardless of whether or not the Nezvorov probe measured a nonzero IWC. On the other hand, the average FSSP PSDs measured in glaciated clouds (medium thick lines) exhibited very broad distributions. Average FSSP concentrations for mixed-phase conditions were 33 ± 25 cm^{-3} and 72 ± 45 cm^{-3} for conditions with IWC > 0 and IWC $= 0$, respectively, as measured with the Nevzorov probe. For comparison, the average FSSP concentrations in glaciated conditions were 0.6 ± 0.6 cm^{-3} for IWC < 0.01 g m^{-3} and 0.9 ± 0.9 cm^{-3} for IWC > 0.01 g m^{-3}, and in liquid-phase conditions, 39 ± 34 cm^{-3} for LWC > 0.005 g m^{-3}. The FSSP PSDs shown in Fig. 2 closely match the observed patterns of Cober et al. (2001a) in liquid-phase clouds. Since the water particles are dominating the mass distribution in the FIRE-ACE mixed-phase clouds and since the observed PSDs of these clouds closely match those of liquid-phase clouds, it suggests that the particles measured by the FSSP are water drops and, hence, the projected areas and mass contents of these particles can be readily calculated using spheres with density 1 g cm^{-3}.

The PSDs for ice clouds are estimated from the 2D data. The 2DC is used to estimate PSDs for particles with X dimensions between 125 and 800 μm, where X represents the maximum diameter of the particle in the time direction parallel to the aircraft motion, and the 2DP is used for particles with X dimensions larger than 800 μm. Figure 3 shows average PSDs estimated from

2D data for several different conditions. For mixed-phase (thickest lines) and ice-phase clouds (lines of medium thickness), particles larger than 125 μm up to 6000 μm are seen in the average PSDs. On the other hand, for liquid clouds (thinnest lines), there are very low number concentrations. Liquid drops larger than 100 μm were identified in only four of the 30-s observations during FIRE-ACE. As expected, larger concentrations and larger particles were observed by 2D probes in mixed-phase clouds when the Nezvorov probe detected nonzero IWCs (solid lines) as opposed to zero IWCs (dashed lines). For ice-phase clouds, average PSDs corresponding to IWCs > 0.01 g m^{-3} (dashed) and IWCs < 0.01 g m^{-3} (solid) are also shown.

d. Shape analysis and mass computations

An automatic shape classification algorithm (Cober et al. 2001a) was used to segregate the 2D images into circles and noncircles. The noncircular particles were further subdivided into irregular, dendritic, and needle shapes following Korolev and Sussman (2000). For ice-phase conditions, where noncircular particles would be expected to dominate, 68% of the particles in the average PSDs were noncircular for IWC < 0.01 g m^{-3}, and 78% for IWC > 0.01 g m^{-3}. For particles with X diameters smaller than 300 μm, only 61% of the ice crystals were classified as having noncircular shapes, whereas 96% of particles larger than 300 μm were classified as noncircular. These observations are consistent with those of Cober et al. (2001a). Many of the smaller ice crystals, while presumably of a noncircular shape, will be classified as circular because of the 25-μm pixel resolution of the 2DC and 2DG probes. For mixed-phase cases with nonzero IWCs estimated by the Nezvorov probe, 82% of all particles in the average PSDs are classified as noncircular, with 73% and 94% of those smaller and larger than 300 μm classified as noncircular. For cases with an IWC $= 0$ g m^{-3} (as measured with the Nevzorov probe), the three percentages listed above are 71%, 60%, and 89%, respectively. This suggests that the characteristics of the larger particles observed by the 2D probes are similar for mixed-phase and ice-phase conditions, implying that the larger particles measured by the 2D probes in mixed-phase conditions can be considered ice.

Figure 4 provides further evidence for this assumption by showing shadows of crystals imaged in mixed-phase conditions. The particles detected include aggregates (e.g., 1931 UTC 15 April), quasi-circular ice (e.g., 1936 UTC 15 April), needles (e.g., 2256 UTC 16 April), mixed drizzle and ice (e.g., 1845 UTC 17 April), and dendrites (e.g., 1926 UTC 21 April). For the 204 thirty-second time periods identified as mixed phase, only 4 were identified as mixed drizzle and ice crystals where liquid particles might make a significant contribution to the 2D particles. The other periods were identified as semicircular ice crystals (62 periods), no dominant ice crystal habit (120 periods), periods where needles dominated (4 periods), and periods where dendrites dominated (15 cases).

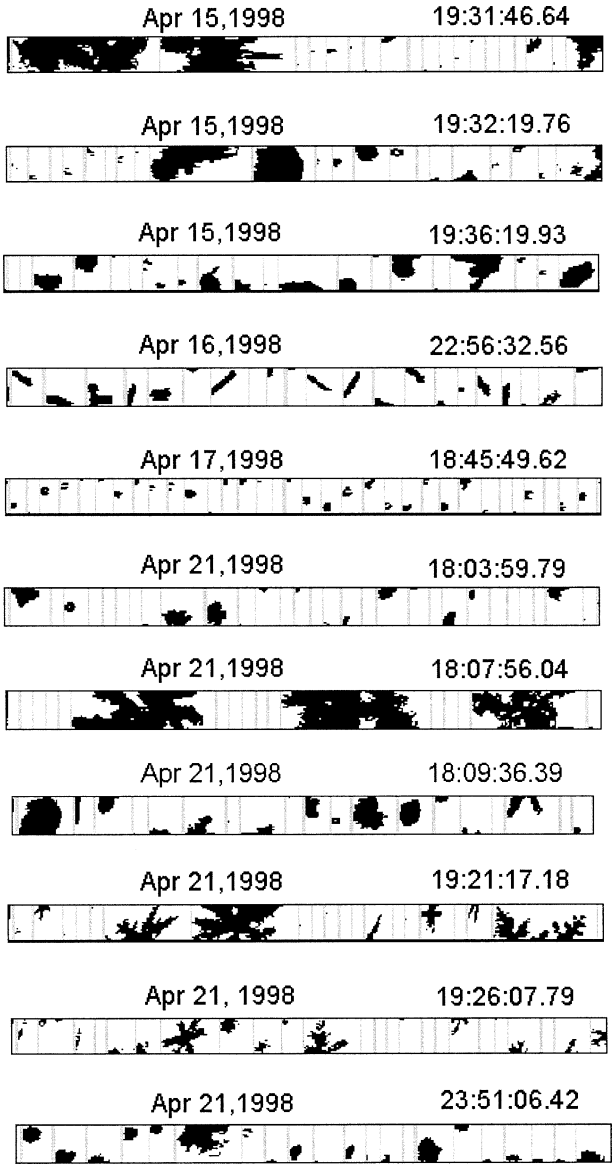

FIG. 4. Crystals imaged by 2D probes in conditions identified as mixed phase by the Cober et al. (2001a) algorithm.

Estimates of particle mass (m) and projected area (A) are required to calculate single-scattering properties of ice particles measured by the 2D probes. For a given shape, m–D and A–D relations (e.g., Mitchell 1996) can be used to estimate these quantities from the crystals' measured dimension. However, given Fig. 4, it is difficult to identify a representative shape to characterize mixed-phase ice crystals, and especially to classify specific shapes for all individual crystals. Korolev et al. (1999) also showed that only 3% of ice particles that they sampled in Arctic clouds had pristine habits; the irregular crystals sampled were either faceted poly-

crystalline particles or sublimating ice particles with smooth edges. For some cases, IWCs estimated using the Nezvorov probe could be used to derive coefficients appropriate to use in the *m–D* relations. However, for 85% of the mixed-phase cases during FIRE-ACE, the IWC estimated in this way was too small to extract from the Nezvorov signal. Hence, an alternative approach was required.

Boudala et al. (2002b) compared IWCs derived from various *m–D* and *A–D* relations (Cunningham 1978; Mitchell et al. 1990; Brown and Francis 1995) against direct measurements from the Nezvorov probe, using data collected with the NRC Convair-580 aircraft in several field campaigns including FIRE-ACE. The different calculations showed considerable variability in the estimated IWCs and Boudala et al. (2002b) suggested that Cunningham's (1978) *m–A* relations best characterized the IWCs measured by the Nezvorov probe. Hence, the Cunningham (1978) coefficients are used in this study to estimate masses for ice crystals measured by 2D probes; the relative fraction of dendrites, circular crystals, needles, and irregular crystals are set according to the fractions calculated for each time period when ice particles were detected. Because the majority of crystals observed during FIRE-ACE shadowed one of the end elements of the photodiode array, reconstruction techniques that assume circular symmetry were used to estimate *A*, giving relatively large uncertainties in measured areas. Hence, it is more desirable to use the particle dimension for calculation of the single-scattering and bulk microphysical properties. For this reason, and to be consistent with the crystal models used for the computation of the single-scattering techniques (Yang et al. 2000) described later, the areas of dendrites, needles, and irregular crystals are first estimated from the crystal models for which the library of single-scattering properties are available and the corresponding measured maximum dimension, and these areas are then used to estimate the particle masses following Cunningham's (1978) approach.

The use of the Cunningham (1978) *m–D* and *A–D* coefficients together with the crystal geometries used to define dendrites, needles, circular, and irregular ice crystals and PSDs estimated from the 2DC and 2DP allows a determination of the mass and area distributions of the ice crystals. These distributions are combined with PSDs measured by the FSSP, which are assumed to represent water drops. Figure 5 shows a scatter diagram of the projected area from liquid particles compared to the total projected area of all particles using the derived distributions for conditions identified as mixed phase. It can be seen that, even when adding contributions of the ice particles that are not well detected by the Nezvorov probe, the area of the mixed-phase clouds are dominated by the liquid particles. This suggests that single-scattering properties of mixed-phase clouds should be dominated by the properties of supercooled water drops. Further, parameterization schemes that assume simple temperature-dependent mixtures of phases may not adequately represent the properties of such clouds.

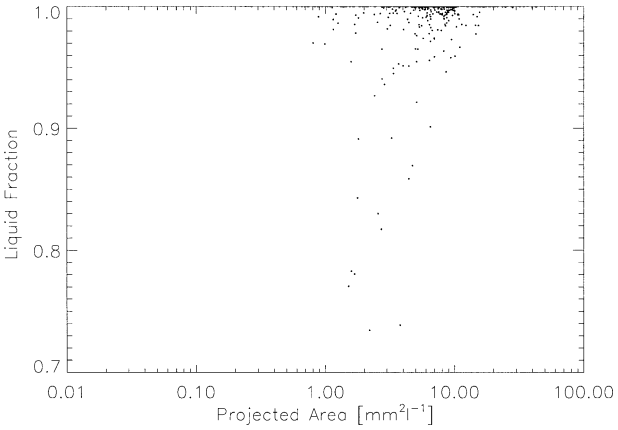

FIG. 5. Fraction of projected area contained in liquid particles as a function of total projected area contained in all phases of particles for all 30-s averaged cloud penetrations identified as mixed phase.

Although a relatively small set of data was used to construct Figs. 5 and 1, a larger set of data shows similar trends (Korolev et al. 2003; Cober et al. 2001a) in the frequency of observed liquid fractions in mixed-phase clouds. For example, Fig. 13 in Cober et al. (2001a) shows that about 50% of the clouds that they sampled under mixed-phase conditions had liquid fractions greater than 80% and that these clouds consisted of relatively large ice crystals and smaller supercooled cloud drops with substantial LWC. They also found that about 15% of their clouds had liquid fractions smaller than 0.2, which were mostly glaciated clouds with a small cloud droplet mode. The absence of any ice-dominated clouds in the mixed-phase population considered here may be a unique feature of Arctic clouds, or may be caused by a small sample size or averaging period.

A large percentage of clouds observed during FIRE-ACE and in the larger sample considered by Cober et al. (2001a) consisted exclusively of ice crystals or supercooled water droplets, even though they occurred in the temperature range where mixed-phase clouds are typically observed, namely between 0° and −30°C. This observation that many clouds are primarily or entirely liquid or ice is inconsistent with the implementation of many parameterizations in large-scale models. These parameterizations frequently determine the single-scattering properties of clouds in this temperature range by weighting the single-scattering properties of water droplets and ice crystals by temperature-dependent estimates of the fraction of liquid water. Hence, for some temperature ranges clouds consist of nearly equal mixtures of water and ice in contrast to the observations. The effect of such assumptions on estimates of cloud radiative forcing needs to be investigated. These calculations are performed in the next section using the ob-

served water and ice PSDs in combination with libraries of single-scattering properties.

3. Calculation of single-scattering properties

The most important single-scattering properties that affect cloud–radiation interactions at the solar wavelengths used in large-scale models are the single-scatter albedo (ω_0), the asymmetry parameter (g), and the extinction cross section (β_{ext}). In order to determine these single-scattering properties for mixed-phase clouds, it is necessary to first know those wavelength and size-dependent properties for the particles that make up the PSDs in mixed-phase clouds.

The single-scattering properties of water droplets are calculated using Mie theory (code supplied by A. Macke) and using the real and refractive indices of refraction provided by Hale and Querry (1972), Ray (1972), Palmer and Williams (1974), and Downing and Williams (1975). For ice crystals, calculations are more complex because the observed ice crystals must be characterized by one of several shapes for which libraries of single-scattering properties are available. Yang et al. (2000) has compiled a library of such properties calculated using an improved geometric ray-tracing method, referred to as GOM2, for the following shapes: smooth aggregates, rough aggregates, bullet rosettes, columns, hollow columns, and plates. Because it is difficult to identify any pristine representative shape for the irregular crystals sampled during FIRE-ACE, the single-scattering properties of rough aggregates are used to represent those of the irregular ice crystals. Although rough aggregates do not perfectly represent the observed crystals, their use produces featureless phase functions that more closely match in situ observations of scattering phase functions (e.g., Garrett et al. 2001) than the use of more pristine habits such as columns or plates. Macke et al. (1996) and Baran et al. (2001) have also produced featureless phase functions through the use of Koch fractal crystals and analytic phase functions respectively, but they are not used here because the former does not resemble any crystals observed in situ and the later requires a priori information about g, knowledge of which is lacking. The real and imaginary parts of the index of refraction for ice are obtained from the works of Warren (1984), Perovich and Govoni (1991), and Kou et al. (1994).

In analogy to the techniques used by Macke et al. (1998) and McFarquhar et al. (2002) to compute the single-scattering properties of mixed size and shape distributions of ice clouds, the single-scattering properties of the mixed-phase clouds are computed by weighting the analogous single-scattering property of individual water droplets or ice crystals by the number concentration and scattering cross section of the individual components. For example, g for mixed-phase clouds is given by

$$g = \frac{\sum_{\text{shape}}\sum_{\text{size}} g_{\text{ice,shape,size}}\beta_{s,\text{ice,shape,size}}n_{\text{ice}}(D_{\text{shape,size}}) + \sum_{\text{size}} g_{\text{wat,size}}\beta_{s,\text{wat,size}}n_{\text{wat}}(D_{\text{size}})}{\sum_{\text{shape}}\sum_{\text{size}} \beta_{s,\text{ice,shape,size}}n_{\text{ice}}(D_{\text{shape,size}}) + \sum_{\text{size}} \beta_{s,\text{wat,size}}n_{\text{wat}}(D_{\text{size}})}, \quad (1)$$

where $g_{\text{ice,shape,size}}$ is the asymmetry parameter for a given shape and size ice crystal, $\beta_{s,\text{ice,shape,size}}$ is the corresponding scattering cross section, n_{ice} is the number concentration of particles with maximum dimension ($D_{\text{shape,size}}$), $g_{\text{wat,size}}$ is the asymmetry parameter for a given size of water droplet, $\beta_{s,\text{wat,size}}$ its scattering cross section, and n_{wat} the number concentration of water droplets with a diameter D_{size}. Similar calculations can be performed to derive ω_0, β_{ext}, the extinction efficiency, Q_e, the scattering efficiency, Q_s, and the scattering phase function, $P(\Theta)$. Separate computations can be done for water or ice components by leaving out the appropriate terms from the summation in Eq. (1).

Single-scattering properties are calculated for all mixed-, liquid-, and ice-phase clouds. For ice-phase clouds, a straightforward observation of size distributions of small ice particles, namely those with maximum dimensions smaller than about 100 μm, is not readily available because it is known how well the FSSP measures small ice particles. McFarquhar and Heymsfield (1996) and others have shown that such crystals may contribute significantly to the radiative properties of ice clouds. For one sensitivity study, it is assumed that the small crystals can be accurately measured by the FSSP, whereas for another sensitivity study, the numbers of small ice crystals is simply set to zero. These two studies will determine single-scattering properties for ice clouds that likely both underestimate and overestimate the importance of small ice crystals. Because other instruments were not available to quantify small particle concentrations [e.g., those used by Arnott et al. (1994) or McFarquhar and Heymsfield (1996) during other experiments], this approach is necessary. Because small ice crystals have been observed to have quasi-spherical shapes, their single-scattering properties are determined following the techniques of McFarquhar et al. (2002), who represented the shapes of small ice crystals by expansions of Chebyshev polynomials.

The temperature dependence of the single-scattering properties calculated for clouds observed during FIRE-

ACE is not examined in this paper because there is not an adequate statistical sample to program such an analysis. The size distributions of clouds derived in section 2 are implemented in the analysis described above to determine typical single-scattering properties of Arctic clouds between 0° and −30°C in the next section.

4. Single-scattering and radiative properties of mixed-phase clouds

a. Derivation of single-scattering properties

In this section, the relative roles of water and ice in determining single-scattering and optical properties of mixed-, liquid-, and ice-phase clouds observed during FIRE-ACE are examined and compared against those properties that would be predicted using parameterization schemes currently implemented in large-scale models. In particular, it is examined whether parameterizations based on average contributions of the different phases can be used to represent radiative fluxes that would be produced by the observed distributions of phases inside clouds. For large-scale models with one prognostic water variable, parameterization schemes are used to estimate the fraction of liquid water that occurs in clouds present in temperature ranges where water and ice can coexist. The single-scattering properties of clouds are then determined using a weighted average of the single-scattering properties of water droplets and ice crystals according to this fraction. For example, such algorithms are used in the Scripps single column model (e.g., Iacobellis et al. 2003, and references contained therein) using the liquid fraction scheme of Smith (1990).

For this paper, the parameterization for liquid fraction used to compute the single-scattering properties, henceforth called parameterized single-scattering properties, is that of Boudala et al. (2002a). This scheme gives the liquid water fraction as a function of temperature and total water content. Although the Boudala et al. (2002a) scheme has not been implemented in any large-scale models, this scheme is used in this analysis because it is based on a set of data that include the FIRE-ACE observations and should presumably give the best possible match against single-scattering properties computed using the FIRE-ACE in situ observations. Similar comparisons could be made against schemes implemented in large-scale models (e.g., Smith 1990), but then issues concerning how well the parameterization scheme represents the average fraction of liquid to total water observed during FIRE-ACE would dominate issues concerning how well a parameterization scheme of average properties, based on observed size and phase distributions, can represent radiative fluxes associated with those same observations.

The single-scattering properties of supercooled water droplets and ice crystals that are combined using the parameterized water fraction are calculated from the water droplets and ice crystals that make up the 30-s averaged distributions for the FIRE-ACE mixed-phase clouds. For clouds exclusively composed of water or ice, parameterized single-scattering properties are still calculated using the parameterized liquid fraction, with the single-scattering properties of the phase not present based on the average properties of that phase observed for other cloud penetrations. Hence, for all in situ distributions measured in mixed-, ice-, or liquid-phase clouds, the parameterized single-scattering properties may be compared against those properties computed using observed size, phase, and shape distributions [e.g., Eq. (1)], which are henceforth called observed single-scattering properties. These include estimates of g, ω_0, and β_{ext}.

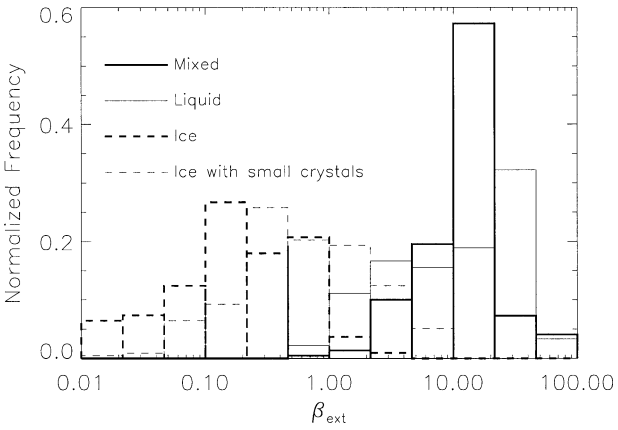

FIG. 6. Normalized distribution of frequency of occurrence of β_{ext} for the 0.25–0.69-μm wavelength band for mixed-, liquid-, and ice-phase clouds with and without the contributions of small ice crystals measured by the FSSP. Curves are normalized so that total number of occurrences for each cloud type is 1.

Figure 6 shows frequency distributions of β_{ext}, corresponding to the wavelength band 0.25 to 0.69 μm, calculated from in situ observations combined with libraries of single-scattering properties, with different line types representing mixed-, liquid-, and ice-phase clouds; for ice clouds, calculations both with and without contributions due to small crystals measured by the FSSP are shown. As expected, optical depths (τ) for water and mixed-phase clouds are larger than those for the ice clouds, even when small ice crystals are assumed to have the maximum contributions that are measured by the FSSP. Figure 7 also shows the fractional contribution of β_{ext} from water droplets for those clouds that have been identified as mixed phase. It can be seen that β_{ext} is dominated by contributions from water droplets, with ice crystals making only minimal contributions to β_{ext}. Asterisks represent the fractional contribution of liquid to β_{ext} that would be predicted from the Boudala et al. (2002a) parameterization scheme. The parameterization scheme predicts that ice contributes substantially larger fractions to β_{ext} in mixed-phase clouds than shown by the observations. Similar discrepancies between ob-

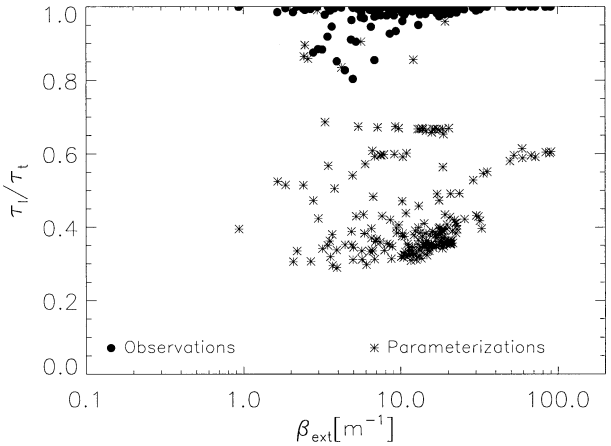

FIG. 7. Fraction of β_{ext} due to liquid particles compared to total β_{ext} as function of total β_{ext} for all cloud penetrations identified as mixed phase. Circles represent calculations using observed PSDs, and asterisks represent calculations using the Boudala et al. (2002a) parameterization of liquid fraction as described in text.

served and parameterized fractions of liquid water to β_{ext} are seen when other parameterizations schemes, such as that of Smith (1990), are used (figure not shown). In fact, for the FIRE-ACE observations, the parameterized liquid water fraction to β_{ext} is consistently a factor of 2 lower than observed. These very different liquid water fractions should also have a substantial impact on other single-scattering properties.

Figure 8 shows the normalized frequency of occurrence of g values calculated from the observations and from the parameterization for four broad bands commonly used in CCM3 and other large-scale models. The different line types represent observed distributions of g for mixed-, liquid-, and ice-phase clouds, and the parameterized distributions. For the two bands at the shortest wavelengths (λ) especially, where the greatest percentage of solar energy is contained, the distributions of g for mixed-phase and liquid-phase clouds are similar. For example, g peaks around 0.85 for mixed-phase clouds for λ between 0.25 and 0.69 μm, and around 0.87 for liquid-phase clouds at the same λ. On the other hand, g for the ice phase and modeled mixtures are around 0.77 for this λ. For the higher λ band of 2.38 to 4.0 μm, the g peaks of 0.85 and 0.89 for mixed- and liquid-phase clouds are lower than the ice and modeled mixture peaks of around 0.93. The similarities between the mixed-phase and liquid-phase g values occur because liquid contributes most to the mass fraction and hence to the scattering of these mixed-phase clouds. The use of Boudala et al.'s (2002a) parameterization for the modeled mixtures gives g closer to the values calculated for ice clouds because larger fractions of ice are calculated with this parameterization for some temperatures.

This does not mean that the parameterization is inconsistent with the observations, rather that this scheme is based on a statistical average of the contributions of liquid and ice obtained from cloud penetrations that included clouds entirely made of water and ice. It is not surprising that clouds that are entirely mixed phase exhibit different behavior.

Figure 9 shows a similar analysis for calculations of ω_0, but only for the two longest λ bands where ω_0 is

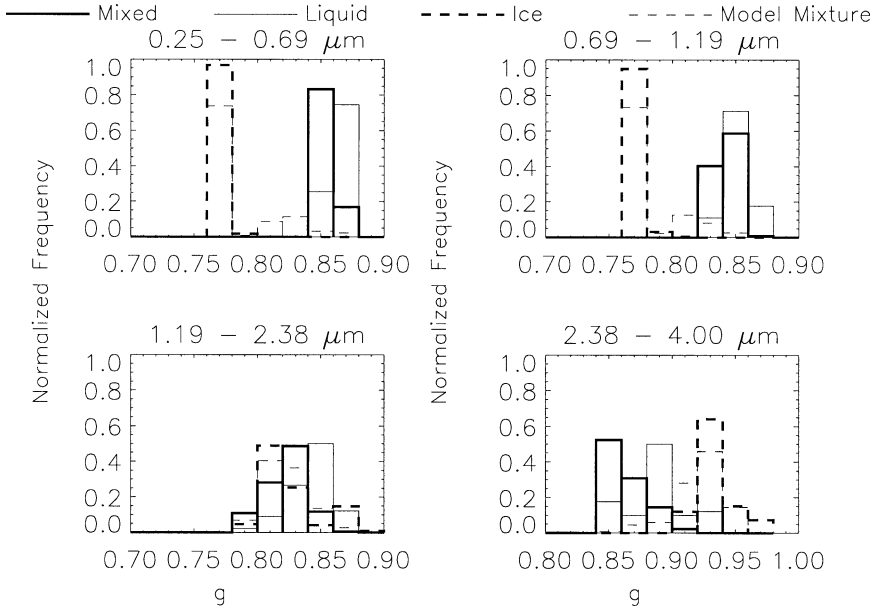

FIG. 8. Normalized frequency distributions of g for four broad bands commonly used in large-scale models. Different line types correspond to frequency distributions for mixed-phase (thick solid), liquid-phase (thin solid), and ice-phase clouds (thick dashed), and for calculations of g using the Boudala et al. (2002a) parameterization of liquid water fraction (thin dashed).

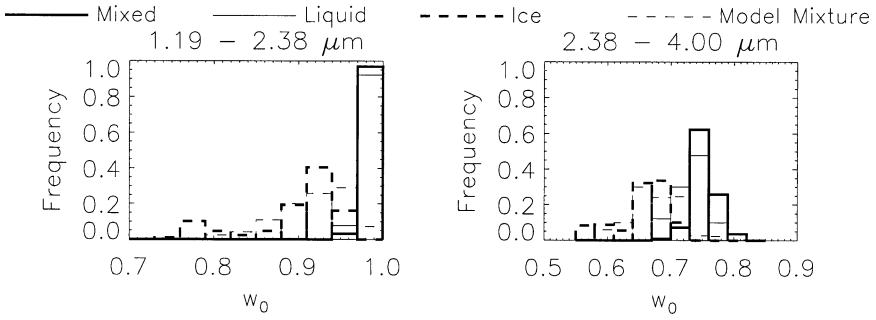

FIG. 9. As in Fig. 8 except for distributions of ω_0 for two highest wavelength bands. Thick solid lines represent frequency distributions for mixed-phase clouds; thin solid, liquid phase; thick dashed, ice phase; thin dashed, Boudala et al. (2002a) parameterization.

not close to unity. As for the distributions of g, the mixed-phase clouds and liquid-phase clouds have very similar distributions, with peak ω_0 of between 0.98 and 1.0 in the 1.19–2.38-μm band and between about 0.74 and 0.76 in the 2.38–4.0-μm band. These are much higher than the values for the ice and the parameterized clouds, which show similarities. More absorption occurs in the ice particles than in the supercooled water droplets partly because of differences in the refractive indices of water and ice, but also partly because the ice crystals typically have larger sizes than the water drops. The water and mixed-phase clouds again have similar ω_0 because of the larger contribution of water than of ice to the calculation of ω_0.

There are other data that show the above trend, of water contributing most to the properties of the mixed-phase clouds, does not occur only for a small sample of mixed-phase clouds, but rather is real and significant. For example, in their Fig. 13, Cober et al. (2001a) show histograms of the frequency of occurrence of liquid water fraction from 2925 mixed-phase clouds sampled during the Canadian Freezing Drizzle Experiments I and III for temperatures between 0° and −30°C. These data are consistent with that presented here in that many cases have liquid fractions greater than 0.8, but only very few cases have relatively equal mixtures of phases, that is, liquid fractions between 0.2 and 0.8. Cober et al. (2001a) also reported that about 13% of the cases had liquid fractions between 0 and 0.2. Such small liquid fractions are not seen in the analysis presented here, possibly because of sampling issues. Thus, the findings shown here regarding the importance of water in determining the single-scattering properties of mixed-phase clouds should apply to all mixed-phase clouds as based on all observational evidence to date.

b. Calculation of radiative fluxes

Differences in g and ω_0 between observed and parameterized mixed-phase clouds are likely large enough to significantly affect estimates of cloud radiative forcing and predicted fluxes at the top of the atmosphere and surface. Vogelman and Ackerman (1995) showed that, to obtain the flux accuracy criteria of ±5% identified as needed for large-scale models, accuracies in g of better than 2% and 5% were needed for τ of 12 and 2, respectively, for g of approximately 0.80. Given typical τ for Arctic clouds and the discrepancies between observed and parameterized g in Fig. 8, the differences seem significant. McFarquhar et al. (2002) also showed that differences in g values of 0.10, larger than those shown in Fig. 8, give significant discrepancies in estimates of radiative fluxes for tropical clouds. To further determine how differences between observed and parameterized single-scattering properties affect the determination of radiative fluxes and cloud–radiative interactions, simulations using a plane-parallel radiative transfer model are conducted as described below.

A plane-parallel radiative transfer simulation is conducted using each PSD observed during FIRE-ACE to construct a vertically and horizontally homogeneous cloud as input to a Monte Carlo radiative transfer program [developed by A. Macke (1994)] that computes fluxes and radiance fields. One million incoming photons were used in each simulation. Sensitivity studies are used to define clouds of varying thickness (500 m, 1 km, 2 km) and varying surface albedo. McFarquhar et al. (1999) showed that assumptions on such quantities significantly impact the calculated radiative fluxes, but here differences in radiative transfer due to varying mixtures of phases are concentrated upon. Separate simulations are conducted using observed and parameterized values of $P(\Theta)$ and ω_0, which are also required as input to the Monte Carlo model. The extinction coefficient was set equal to that calculated using the in situ data and GOM2. It is important to emphasize that β_{ext} and τ were equal for simulations with the observed and parameterized $P(\Theta)$ and ω_0 and that, therefore, differences in calculated radiative fluxes are due only to variations in the scattering and absorption of radiation by otherwise geometrically and optically similar clouds.

To approximate the Arctic environment, a solar zenith angle of 60° was assumed in these calculations. It is more difficult to determine a representative surface albedo for FIRE-ACE conditions as Minnis et al. (2001)

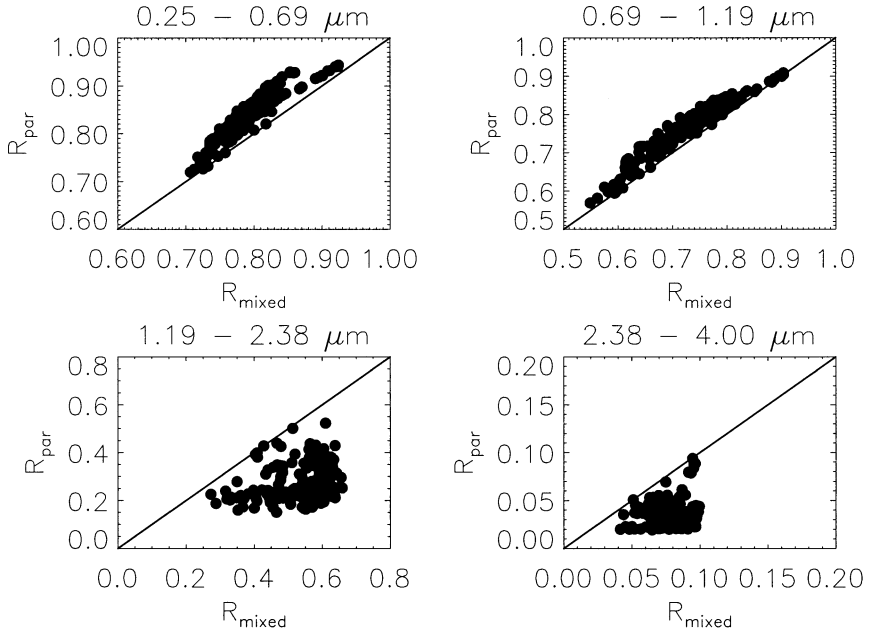

FIG. 10. Albedo computed using plane-parallel model assuming 1-km-thick cloud and single-scattering properties determined from observations of mixed-phase clouds during FIRE-ACE on horizontal axis vs albedo determined from parameterized single-scattering properties on vertical axis. Each point represents calculation from 30-s time average of in situ measurements.

and Doelling et al. (2001) found that clear sky albedos varied considerably depending on solar zenith angle, snow conditions, and the variability in the Arctic surface. Cloud temperatures are similar to surface temperatures, further complicating such estimates. For this study, typical snow albedos of 0.7 (0.25 to 0.69 μm), 0.5 (0.69 to 1.19 μm), 0.1 (1.19 to 2.38 μm), and 0.05 (2.38 to 4.0 μm) are used and a Lambertian surface is assumed. An additional set of simulations with lower albedos in visible channels of 0.4 (0.25 to 0.69 μm) and 0.3 (0.69 to 1.19 μm), corresponding to reduced snow cover, are also performed. Molecular and aerosol scattering and absorption are not considered in this conceptual study. This strategy allows an examination of impacts on assumptions about phase mixtures on calculated radiative fluxes over a broad range of conditions approximating the Arctic environment.

Figure 10 shows top of the atmosphere albedo in four solar broad bands calculated using the plane-parallel model assuming 1-km-thick clouds with β_{ext}, ω_0, and $P(\Theta)$ computed following techniques presented in the previous section for the observed clouds that were identified as mixed phase on the horizontal axis, with albedo in the same four bands calculated with the same β_{ext}, but using the parameterized ω_0 and $P(\Theta)$ as input to the plane-parallel model on the vertical axis. For shorter λ, albedos calculated using the parameterized single-scattering properties are consistently higher than those determined using the in situ observations. For example, for the 0.25–0.69-μm band, the average albedo calculated using observed single-scattering properties was 0.80, or 6% lower than the average albedo of 0.85 for parameterized single-scattering properties. This occurs because water droplets play a larger role in determining the single-scattering properties of observed clouds than of parameterized clouds, where ice typically plays a larger role. Although ω_0 are close to unity for both water and ice in visible bands, g values are larger for water droplets than for ice crystals, meaning that more radiation is scattered in the forward direction for water droplets than for ice crystals. Hence, for the in situ distributions with a greater contribution of water, the radiation scattered in the backward direction is less.

For longer λ, albedos from parameterized clouds are substantially lower than those from the observed clouds. For example, for the 1.19–2.38- and 2.38–4.0-μm bands, the average albedo varies from 0.55 and 0.079 for the observed single-scattering properties to 0.28 and 0.034 for the parameterized single-scattering properties, representing differences of almost a factor of 2. Differences are associated with variations between ω_0 for water and ice: ice crystals absorb more radiation than supercooled water at these wavelengths, mainly because of their larger sizes. Hence, reflection is reduced for parameterized clouds that have a greater fraction of ice because of increased absorption. The differences in albedo are significant given the flux accuracy criterion expressed by Vogelman and Ackerman (1995) and McFarquhar et al. (2002). Differences in cloud heating rate associated with the variations in ω_0 and $P(\Theta)$ would also impact processes occurring in cloud and hence affect the amount of cloud water gained or lost within

TABLE 1. Average albedo computed at top of the atmosphere (TOA) for different λ bands using different estimates of surface albedo (ground) for solar zenith angle 60°. Different albedos correspond to simulations conducted using observed single-scattering properties and parameterized single-scattering properties.

		R (TOA)	
λ (μm)	R (ground)	Observed	Parameterized
0.25 to 0.69	0.70	0.75	0.77
0.69 to 1.19	0.50	0.64	0.65
1.19 to 2.38	0.10	0.36	0.24
2.38 to 4.00	0.05	0.059	0.045
0.25 to 0.69	0.40	0.58	0.61

cloud. McFarquhar et al. (2003) showed that such feedbacks on cloud amount and cloud water could be just as important as differences in single-scattering properties in determining cloud radiative feedbacks and in estimating cloud radiative forcing.

Although differences in albedos for clouds constructed with observed and parameterized single-scattering properties are informative, the most important climatic issue is determining how to represent single-scattering properties of distributions of clouds that contain varying mixtures of phases over the large spatial scales representative of grid boxes in GCMs, on the order of 100 km. Over such scales, there will be mixtures of mixed-, ice-, and water-phase clouds at temperatures between approximately 0° and −30°C. To test how well the Boudala et al. (2002a) scheme calculates the single-scattering properties of cloud distributions, the average albedo determined using all FIRE-ACE cloud observations, including ice- and liquid-phase clouds, was compared against the average albedo calculated using the observed total water contents and the parameterized single-scattering properties. This differs from the simulations depicted in Fig. 10 in that all clouds observed during FIRE-ACE are considered, rather than just mixed-phase clouds. Although the FIRE-ACE data obtained at multiple locations on different days might encompass more variability than might be contained in a typical 100 km by 100 km GCM grid box at a single instance in time, data sampling rates prevent enough data being obtained to test the mixing hypothesis in a single grid box at a specific time.

Table 1 compares the average albedo in four broad bands computed from the observed scattering properties against that calculated using the parameterized scattering properties, where the averages are computed over all mixed-, liquid-, and ice-phase clouds. For the shorter λ bands, when using relatively high surface albedos corresponding to typical snow-covered surfaces, the agreement between simulations using observed and parameterized scattering properties is good, as differences in albedo are less than the 5% accuracy criterion identified. For a lower surface albedo of 0.4 in visible channels, the difference between average albedo is around 5%, very close to the accuracy criteria identified by Vogelman and Ackerman (1995). For lower λ, the differences are more significant; however, because the majority of solar radiation occurs at lower wavelengths, these differences might not impact the radiative budget as much. On the other hand, there would be a greater impact on the value of effective particle size retrieved from satellite algorithms because the near-infrared wavelengths are used to retrieve these sizes.

The experiments in Fig. 10 and Table 1 reach seemingly contradictory conclusions about the ability of parameterizations used in large-scale models to represent the single-scattering properties of mixed-phase clouds, especially when considering cases with higher surface albedos. The differences occur because of the scales over which the comparisons are performed, from small scales in Fig. 10 to larger scales from the averages compared in Table 1. Differences in Fig. 10 would be more significant if the occurrence of clouds with particular phases was clustered, meaning that, if a 30-s average cloud distribution were obtained in a mixed-phase clouds, the neighboring clouds would more likely be mixed phase. Analysis of the FIRE-ACE data shows that this is exactly the case; over 90% of the 30-s average sized distributions identified as mixed phase occurred either before or after another mixed-phase cloud distribution.

Because differences in cloud radiative forcing, and hence in cloud heating rates, exist in the smaller scales represented by Fig. 10 and because the phases of the clouds tend to be clustered, these differences could naturally feed back on the temporal evolution of the cloud. Thus, even though the top of the atmosphere albedo might not be significantly overestimated by the parameterization in an average sense, there could still be large impacts on the evolution of cloud fields and, hence, on the estimated cloud radiative impacts. Thus, further knowledge of the scales over which mixing occurs is critically needed for future studies of mixed-phase clouds.

5. Conclusions

In situ observations of the sizes, shapes, and phases of cloud particles obtained during FIRE-ACE have been used to investigate the single-scattering and radiative properties of Arctic mixed-phase clouds. Consistent with previous studies, it has been found that mixed-phase clouds occur frequently and that supercooled water droplets typically dominate the mass contents of such clouds. This study has focused on the radiative impacts of such phase mixing by examining the relative roles of water and ice in determining the single-scattering properties of mixed-phase clouds. Radiative transfer simulations, conducted with a plane-parallel model, have then been used to investigate whether conventional parameterization schemes accurately predict the radiative fluxes that would be expected to be associated with such clouds. The particular conclusions of this study can be summarized as follows:

1) For clouds sampled in situ during FIRE-ACE, 33% were identified as mixed phase, and 16% and 51% were identified as liquid and ice phase, respectively. Of the mixed-phase clouds, 87% had over 90% of the mass content contained in supercooled water droplets.
2) The single-scattering properties of the clouds sampled during FIRE-ACE were determined using the size and shape distributions observed, in conjunction with a library of single-scattering properties calculated using Mie theory for water droplets and an improved geometric ray-tracing technique.
3) Substantial differences were noted between the single-scattering phase functions of mixed-phase and ice-phase clouds, even when an upper bound was used for the possible influence of quasi-spherical solid ice particles. Average g for visible bands of mixed-phase clouds are approximately 0.85 and about 0.75 for ice-phase clouds. There are no substantial differences between g for mixed-phase and liquid-phase clouds because of the large contribution of supercooled water to the total mass content.
4) Average ω_0 for ice-phase clouds at near-infrared wavelengths are between 15% and 30% lower than those of mixed-phase clouds because ω_0 for large ice crystals are substantially lower than ω_0 for smaller supercooled water droplets.
5) The albedos computed from a plane-parallel model using the in situ observations are overestimated by albedos computed using conventional mixed-phase parameterizations by an average of 12%; on the other hand, in the near-infrared albedos from the in situ data are underestimated by a factor of 22% from those computed using the parameterizations.
6) For the population of all clouds measured in situ in the Arctic, the albedos averaged over all cases are only estimated incorrectly by a factor of 2% at visible wavelengths when compared against those predicted by the mixed-phase parameterizations used in some large-scale models.
7) Over 90% of mixed-phase clouds occurred immediately adjacent to other mixed-phase clouds. This suggests that the mixed-phase clouds are clustered, suggesting that the 2% average difference in the above albedo underestimates the problems associated with current mixed-phase parameterizations.

Therefore, for temperature ranges where water and ice may coexist, an accurate representation of not only the average liquid fraction of clouds, but also of the probability distribution of liquid fraction and the nature of phase clustering is needed for implementation in large-scale models. However, there have been relatively few reported in situ characterizations of mixed-phase clouds, especially in the Arctic. Knowledge about the clustering or scales over which the different phases mix is especially lacking. This study highlights the importance of obtaining a better dataset in order to improve knowledge about the processes by which the mixing of the different phases occurs because the nature of this mixing can critically impact the single-scattering properties of the clouds, and hence the cloud radiative heating profiles and the temporal evolution of the cloud systems. The database examined here highlighted the importance of the mixing and its impact on the top of the atmosphere albedo, but there were insufficient data to state how the mixing occurred within individual clouds and how it evolved with time. Knowledge of how anthropogenic perturbations to the Arctic system impact ice and water nucleation, and the distribution of mixed-phase clouds, is also required.

In some more recent versions of large-scale models, separate prognostic variables for water and ice have been included (e.g., Rotstayn et al. 1999), negating the need for the implementation of parameterizations like those of Boudala et al. (2002a). However, models with single prognostic water variables are still used. It is also critical that model simulations that use either one or two prognostic variables be statistically compared against observational databases to assess how well the models represent physical processes occurring within clouds. This is important because recent modeling studies (e.g., Harrington et al. 1999; Jiang et al. 2000; Lohmann 2002) have suggested that mixed-phase stratus are sensitive to even minor changes in the number of ice nuclei, a property that has not been well quantified. Thus, more observations of Arctic mixed-phase clouds, a better understanding of the physical processes producing them, and the development of more physically based parameterizations for large-scale models are critically needed.

Acknowledgments. This research was supported by the Department of Energy Atmospheric Radiation Measurement Program (ARM) under Contract DE-FG03-02ER63337, Wanda Ferrell program manager. The cloud microphysical data collected with the Canadian CV580 were obtained from the NASA Langley Research Center Atmospheric Sciences Data Center. The Canadian participation in FIRE-ACE was financially supported by the Panel on Energy Research and Development, the National Research Council, and the Meteorological Service of Canada. The use of the Mie code from Andreas Macke is acknowledged as well as the database of single-scattering properties for pristine crystals, obtained from Ping Yang. The assistance of Gong Zhang in figure preparation is acknowledged. Comments on the manuscript from Larry DiGirolamo and Faisal Boudala were appreciated, as well as thoughtful reviews by Xiquan Dong and an anonymous reviewer.

REFERENCES

Arnott, W. P., Y. Dong, J. Hallett, and M. R. Poellot, 1994: Role of small ice crystals in radiative properties of cirrus: A case study, FIRE II, November 22, 1991. *J. Geophys. Res.,* **99,** 1371–1381.

Baran, A. J., P. N. Francis, L.-C. Labonnote, and M. Doutriaux-Boucher, 2001: A scattering phase function for ice cloud: Tests

of applicability using aircraft and satellite multi-angle multi-wavelength radiance measurements of cirrus. *Quart. J. Roy. Meteor. Soc.*, **127,** 2395–2416.

Borovikov, A. M., L. I. Gaivoronskii, E. G. Zak, V. V. Kostarev, I. P. Mazin, V. E. Minervin, A. K. Khrgian, and S. M. Shmeter, 1963: *Cloud Physics*. Israel Program for Scientific Translations, 392 pp.

Boudala, F. S., G. A. Isaac, S. G. Cober, Q. Fu, and A. V. Korolev, 2002a: Parameterization of liquid fraction in terms of temperature and cloud water content in stratiform mixed phase clouds. Preprints, *11th Conf. on Cloud Physics*, Ogden, UT, Amer. Meteor. Soc., CD-ROM, 2.5.

——, ——, Q. Fu, and S. G. Cober, 2002b: Parameterization of effective ice particle size for high-latitude clouds. *Int. J. Climatol.*, **22,** 1267–1284.

Bower, K. N., S. J. Moss, D. W. Johnson, T. W. Choularton, J. Latham, P. R. A. Brown, A. M. Blyth, and J. Cardwell, 1996: A parameterization of the ice water content observed in frontal and convective clouds. *Quart. J. Roy. Meteor. Soc.*, **122,** 1815–1844.

Brown, P. R. A., and P. N. Francis, 1995: Improved measurement of the ice water content in cirrus using a total water evaporator. *J. Atmos. Oceanic Technol.*, **12,** 410–414.

Cober, S. G., G. A. Isaac, A. V. Korolev, and J. W. Strapp, 2001a: Assessing cloud-phase conditions. *J. Appl. Meteor.*, **40,** 1967–1983.

——, ——, and J. W. Strapp, 2001b: Characterizations of aircraft icing environments that include supercooled large drops. *J. Appl. Meteor.*, **40,** 1984–2002.

Cunningham, M. R., 1978: Analysis of particle spectral data from optical array (PMS) 1D and 2D sensors. Preprints, *Fourth Symp. on Meteorological Observation and Instrumentation*, Denver, CO, Amer. Meteor. Soc., 345–350.

Curry, J. A., and Coauthors, 2000: FIRE Arctic Clouds Experiment. *Bull. Amer. Meteor. Soc.*, **81,** 5–29.

Del Genio, A. D., M.-S. Yao, W. Kovari, and K. K.-W. Lo, 1996: A prognostic cloud water parameterization for climate models. *J. Climate*, **9,** 270–304.

Doelling, D. R., P. Minnis, D. A. Spangenberg, C. Venkatesan, A. Mahesh, F. P. J. Valero, and S. Pope, 2001: Cloud radiative forcing during FIRE ACE derived from AVHRR data. *J. Geophys. Res.*, **106,** 15 279–15 296.

Dong, X., and G. G. Mace, 2003: Arctic stratus cloud properties and radiative forcing derived from ground-based data collected at Barrow, Alaska. *J. Climate*, **16,** 445–461.

Downing, H. D., and D. Williams, 1975: Optical constants of water in the infrared. *J. Geophys. Res.*, **80,** 1656–1661.

Fleishauer, R. P., V. E. Larson, and T. H. Vonder Harr, 2002: Observed microphysical structure of midlevel, mixed-phase clouds. *J. Atmos. Sci.*, **59,** 1779–1804.

Gardiner, B. A., and J. Hallett, 1985: Degradation of in-cloud forward scattering spectrometer probe measurements in the presence of ice particles. *J. Atmos. Oceanic Technol.*, **2,** 171–180.

Garrett, T. J., P. V. Hobbs, and H. Gerber, 2001: Shortwave, single-scattering properties of Arctic ice clouds. *J. Geophys. Res.*, **106,** 15 155–15 172.

Gerber, H., Y. Takano, T. J. Garrett, and P. V. Hobbs, 2000: Nephelometer measurements of the asymmetry parameter, volume extinction coefficient, and backscatter ratio in Arctic clouds. *J. Atmos. Sci.*, **57,** 3021–3034.

Gregory, D., and D. Morris, 1996: The sensitivity of climate simulations to the specification of mixed phase clouds. *Climate Dyn.*, **12,** 641–651.

Hale, G., and M. Querry, 1972: Optical constants of water in the 200 nm to 200 μm wavelength region. *Appl. Opt.*, **12,** 555–563.

Harrington, J. Y., T. Reisin, W. R. Cotton, and S. M. Kreidenweis, 1999: Cloud resolving simulations of Arctic stratus. Part II: Transition-season clouds. *Atmos. Res.*, **55,** 45–75.

Heymsfield, A. J., 1993: Microphysical structures of stratiform and cirrus clouds. *Aerosol–Cloud–Climate Interactions*, P. V. Hobbs, Ed., Academic Press, 97–121.

Hobbs, P. V., A. L. Rangno, M. Shupe, and T. Uttal, 2001: Airborne studies of cloud structures over the Arctic Ocean and comparisons with retrievals from ship-based remote sensing measurements. *J. Geophys. Res.*, **106,** 15 029–15 044.

Iacobellis, S. F., G. M. McFarquhar, D. Mitchell, and R. C. J. Somerville, 2003: On the sensitivity of radiative fluxes to parameterized cloud microphysics. *J. Climate*, **16,** 2979–2996.

Jiang, H., W. R. Cotton, J. O. Pinto, J. A. Curry, and M. J. Weissbluth, 2000: Clould resolving simulations of mixed-phase Arctic stratus observed during BASE: Sensitivity to concentration of ice crystals and large-scale heat and moisture advection. *J. Atmos. Sci.*, **57,** 2105–2117.

Korolev, A. V., and B. Sussman, 2000: A technique for classification of cloud particles. *J. Atmos. Oceanic Technol.*, **17,** 1048–1057.

——, W. J. Strapp, and G. A. Isaac, 1998: The Nevzorov airborne hot-wire LWC–TWC probe: Principle of operation and performance characteristics. *J. Atmos. Oceanic Technol.*, **15,** 1495–1510.

——, G. A. Isaac, and J. Hallett, 1999: Ice particle habits in Arctic clouds. *Geophys. Res. Lett.*, **26,** 1299–1302.

——, ——, S. G. Cober, J. W. Strapp, and J. Hallett, 2003: Observations of the microstructure of mixed phase clouds. *Quart. J. Roy. Meteor. Soc.*, **129,** 39–65.

Kou, L., D. Labrie, and P. Chylek, 1994: Refractive indices of water and ice in the 0.65 to 2.5 micron spectral range. *Appl. Opt.*, **32,** 3531–3540.

Lane, D. E., J. O. Pinto, and J. A. Curry, 2001: Evaluation of GCM radiation codes using SHEBA data. Preprints, *Sixth Conf. on Polar Meteorology and Oceanography*, San Diego, CA, Amer. Meteor. Soc., 285–288.

Lawson, R. P., B. A. Baker, C. G. Schmidt, and T. L. Jensen, 2001: An overview of microphysical properties of Arctic clouds observed in May and July 1998 during FIRE ACE. *J. Geophys. Res.*, **106,** 14 989–15 014.

Li, Z.-X., and H. Le Treut, 1992: Cloud–radiation feedbacks in a general circulation model and their dependence on cloud modeling assumptions. *Climate Dyn.*, **7,** 133–139.

Lohmann, U., 2002: A glaciation indirect effect caused by soot aerosols. *Geophys. Res. Lett.*, **29,** 1052, doi:10.1029/2001GL014357.

——, and E. Roeckner, 1996: Design and performance of a new cloud microphysics scheme developed for the ECHAM general circulation model. *Climate Dyn.*, **12,** 557–572.

Macke, A., J. Mueller, and E. Raschke, 1996: Single scattering properties of atmospheric ice crystals. *J. Atmos. Sci.*, **53,** 2813–2825.

——, P. N. Francis, G. M. McFarquhar, and S. Kinne, 1998: The role of ice particle shapes and size distributions in the single scattering properties of cirrus clouds. *J. Atmos. Sci.*, **55,** 2874–2883.

McFarquhar, G. M., and A. J. Heymsfield, 1996: Microphysical characteristics of three cirrus anvils sampled during the Central Equatorial Pacific Experiment (CEPEX). *J. Atmos. Sci.*, **53,** 2401–2423.

——, ——, A. Macke, J. Iaqunita, and S. M. Aulenbach, 1999: Use of observed ice crystal sizes and shapes to calculate mean-scattering properties and multispectral radiances: CEPEX April 4, 1993, case study. *J. Geophys. Res.*, **104,** 31 763–31 779.

——, P. Yang, A. Macke, and A. J. Baran, 2002: A new parameterization of single scattering solar radiative properties for tropical anvils using observed ice crystal size and shape distributions. *J. Atmos. Sci.*, **59,** 2458–2478.

——, S. Iacobellis, and R. C. J. Somerville, 2003: SCM simulations of tropical ice clouds using observationally based parameterizations of microphysics. *J. Climate*, **11,** 1643–1664.

Minnis, P., and Coauthors, 2001: Cloud coverage and height during FIRE ACE derived from AVHRR data. *J. Geophys. Res.*, **106,** 15 215–15 232.

Mitchell, D. L., 1996: Use of mass- and area-dimensional power laws for determining precipitation particle terminal velocities. *J. Atmos. Sci.*, **53,** 1710–1723.

——, R. Zhang, and R. Pitter, 1990: Mass-dimensional relationship

for ice particles and the influence of riming on snowfall rates. *J. Appl. Meteor.*, **29,** 153–163.
Moss, S. J., and D. W. Johnson, 1994: Aircraft measurements to validate and improve numerical model parameterizations of ice to water ratios in clouds. *Atmos. Res.*, **34,** 1–25.
Palmer, K. F., and D. Williams, 1974: Optical properties of water in the near infrared. *J. Opt. Soc. Amer.*, **64,** 1107–1110.
Perovich, D., and J. Govoni, 1991: Absorption coefficients of ice from 250 to 400 nm. *Geophys. Res. Lett.*, **18,** 1233–1235.
Rangno, A. L., and P. V. Hobbs, 2001: Ice particles in stratiform clouds in the Arctic and possible mechanisms for the production of high ice concentrations. *J. Geophys. Res.*, **106,** 15 065–15 075.
Ray, P. S., 1972: Broadband complex refractive indices of ice and water. *Appl. Opt.*, **11,** 1836–1844.
Rotstayn, L. D., B. F. Ryan, and J. J. Katzfey, 2000: A scheme for calculation of the liquid fraction in mixed-phase stratiform clouds in large-scale models. *Mon. Wea. Rev.*, **128,** 1070–1088.
Shupe, M. D., T. Uttal, S. Y. Matrosov, and A. S. Frisch, 2001: Cloud water contents and hydrometeor sizes during the FIRE Arctic clouds experiment. *J. Geophys. Res.*, **106,** 15 015–15 028.
Smith, R. N. B., 1990: A scheme for predicting layer clouds and their water content in a general circulation model. *Quart. J. Roy. Meteor. Soc.*, **116,** 435–460.
Sun, Z., and K. P. Shine, 1994: Studies of the radiative properties of ice and mixed-phase clouds. *Quart. J. Roy. Meteor. Soc.*, **120,** 111–137.
——, and ——, 1995: Parameterization of ice cloud radiative properties and its application to the potential climatic importance of mixed-phase clouds. *J. Climate*, **8,** 1874–1888.
Vogelman, A. M., and T. P. Ackerman, 1995: Relating cirrus cloud properties to observed fluxes: A critical assessment. *J. Atmos. Sci.*, **52,** 4285–4301.
Warren, S., 1984: Optical constants of ice from the ultraviolet to the microwave. *Appl. Opt.*, **23,** 1206–1225.
Yang, P., K. N. Liou, K. Wyser, and D. Mitchell, 2000: Parameterization of the scattering and absorption properties of individual ice crystals. *J. Geophys. Res.*, **105,** 4699–4718.